W&M ScholarWorks

5-2017

The Mechanism of NMDA Receptor Mediated Increased in Gamma Oscillation Frequency

Prajal Bishwakarma
College of William and Mary

The Mechanism of NMDA Receptor Mediated Increase in Gamma Oscillation Frequency

A thesis submitted in partial fulfillment of the requirement

for the degree of Bachelor of Science in Neuroscience from

The College of William and Mary

by

Prajal Bishwakarma

Accepted for   _____

_____

Dr. Mainak Patel, M.D., Ph.D.

_____

Dr. William Buchser, Ph.D.

_____

Dr. Greg Smith, Ph.D.

Williamsburg, VA

May 3rd, 2015

Abstract

Activation of N-methyl-D-aspartate (NMDA) receptors has been shown to increase the frequency of gamma oscillations in the CA3 region of the hippocampus. The underlying mechanism of the increase however, is unclear. This project utilizes an integrate-and-fire model of the CA3, based on experimental data, to investigate the increase in oscillation frequency. The model was built first without NMDA receptors to simulate carbachol induced oscillations *in vitro.* Then, NMDA receptors were added to evoke the increase in oscillation frequency. The model shows that a shift in mechanism, from a pyramidal neuron-interneuron feedback loop, to interneuron-interneuron oscillations, is responsible for the increase in gamma oscillation frequency. An interesting relationship between the active NMDA mediated current and instantaneous cycle frequencies points to further areas of study.

Acknowledgements

Introduction

Gamma Oscillations

Network oscillations are crucial for neural function (Buzsaki et al., 2004). Different types of oscillations are categorized based on their frequency ranges. For example, delta oscillations occupy the 1.4-4Hz band, theta oscillations occupy the 4-10Hz band, and beta oscillations occupy the 10-30Hz band (Buzsaki et al., 2004). Gamma oscillations, characterized by their 30-90Hz frequencies, have been linked to various neural processes (Buzsaki et al., 2012). For example, gamma oscillations have been implicated in information routing. Different frequencies of incoming gamma oscillations synchronized neurons in the CA1 region of the hippocampus with the CA3 region and the medial entorhinal cortex (Colgin et al., 2009). Gamma oscillations have also been linked to the processing of visual stimuli, and visual working memory (Tallon-Baudry et al., 1999; Busch et al., 2004; Honkanen et al., 2014) Furthermore, gamma oscillations are involved in attention (Bauer et al., 2004; Börgers et al., 2008) and memory (Howard et al., 2003; Sederberg et al., 2007).

The CA3 Region

Gamma oscillations are prominent in the hippocampus (Csicsvari et al., 2003; Lasztóczi et al., 2014). They arise spontaneously in the CA3 region (Hájos et al., 2009) and propagate to the CA1 region (Csicsvari et al., 2003; Montgomery et al., 2007; Zemankovics et al., 2013). The CA3 sub region of the hippocampus consists of excitatory pyramidal cells and inhibitory interneurons. The principal cells of the CA3 region are the glutamatergic pyramidal cells (Andersen, Morris, Amaral, Bliss, & O'Keefe, 2007). Pyramidal cells provide the main output from the CA3 region to the CA1 region via Schaeffer collaterals. Pyramidal cells also provide excitation to the vastly outnumbered interneurons in the CA3. Interneuron subtypes such as the

basket, chandelier, and bistratified cells receive excitatory input from pyramidal cells with a high degree of convergence (Andersen et al., 2007). The interneurons synapse back onto the pyramidal cells, providing gamma-amino butyric acid (GABA) mediated inhibition. One interesting subtype is the interneuron-selective interneurons. Their defining characteristic is that "their axons terminate exclusively on other interneurons" (Andersen et al., 2007, p.70). This creates an interesting network scheme in which the main source of inhibition in the network inhibits itself.

The main external sources of excitation to the CA3 pyramidal cells and interneurons are mossy fibers and the perforant path (Witter, 2007). Mossy fibers are the projections of the granule cells located in the dentate gyrus (Cherubini and Miles, 2015) and the perforant path inputs are the projections of cells in the entorhinal cortex (Andersen et al., 2007). This architecture of the CA3 region forms a feedforward inhibitory structure. Pyramidal cells receive monosynaptic excitation from the mossy fibers and perforant path, and they receive disynaptic inhibition from interneurons. The inhibition arrives with a time lag due to the time course for interneurons to be activated by external input, as well as latency in the interneuron-pyramidal cell synapses (Cherubini and Miles, 2015). Both excitatory and inhibitory synapses in the CA3 exhibit fast kinetics (Geiger et al., 1999; Whittington et al., 2000; Bartos et al., 2002; Bartos et al., 2007).

At GABAergic synapses in the CA3 region, post synaptic inhibition is mediated by the $GABA_A$ receptor. The $GABA_A$ receptor family is composed of 16 different subunits, α_{1-6}, β_{1-3}, γ_{1-3}, δ, ε, π, and θ (Möhler, 2006). The receptor consists of five of the sixteen subunits arranged around a central pore, which forms the channel through which ions diffuse (Möhler, 2006). Upon activation, the $GABA_A$ receptor channel causes an influx of chloride ions, hyperpolarizing the

post synaptic cell (MacDonald et al., 1989, MacDonald and Olsen, 1994). $GABA_A$ receptor channels display fast kinetics (Bartos et al., 2002), allowing for fast inhibition in the CA3. Similarly, the α-amino-3-hydroxy-5-methyl-4-isoxazolepropionic acid (AMPA) receptor mediates fast post synaptic excitation. Activation of AMPA receptors by glutamate causes an influx of sodium ions, depolarizing the postsynaptic cell (McBain et al., 1993). AMPA receptors operate on a fast time scale; they open quickly and close quickly, allowing for rapid and phasic excitation (McBain et al., 1993, Sprutson et al., 1995).

In addition to the AMPA and $GABA_A$ receptor channels, both pyramidal and interneurons in the CA3 express N-methyl-D-aspartate (NMDA) receptors (Monyer et al., 1994; Nakazawa et al., 2002; Nakazawa et al., 2003; Mann and Mody, 2010) . Activated by glutamate, NMDA receptors mediate a tonic excitatory current that decays slowly over several hundred milliseconds (Bartos et al., 2002; Mann & Paulsen, 2007). NMDA receptors consist of a magnesium ion that blocks the ion channel pore. When the membrane potential of the neuron is sufficiently depolarized, the magnesium block opens, causing an influx of calcium and sodium ions (Cull-Candy et al., 2001). The slow kinetics of the closing of the NMDA receptor channel contributes to the long timescale of the resulting excitatory current (Mann and Mody, 2010).

The CA3 region also exhibits recurrent synapses between pyramidal neurons and interneurons (Bains et al., 1999; Wittner et al., 2006; Cherubini and Miles, 2015). As illustrated in Fig.1, pyramidal neurons synapse onto other pyramidal neurons as well as interneurons (Hasselmo et al., 1995; Andersen et al., 2007). The recurrent synapses allow for synchronous firing of neurons in the CA3 (Miles et al., 1988; Bains et al., 1999). Synchronous firing of pyramidal cells induces excitatory post synaptic currents, increasing the membrane potentials of post synaptic neurons. Interneurons on the other hand, induce inhibitory post synaptic currents,

decreasing the membrane potentials. These rhythmic fluctuations of cellular membrane

potentials are easily observable in the field potential of large populations of cells (Bartos et al.,

2007).

Generation of Gamma Oscillations

There are two mainstream models that outline the generation of gamma oscillations. The

first, named the "I-I model" by Buzsáki et al. in their 2012 review, attributes the production of

oscillations to the mutual connections between interneurons. When the interneurons receive tonic

excitation, a subgroup of the neurons fire synchronously, inhibiting the rest of the population.

When the inhibition wears off, the rest of the population spikes, inhibiting the first subgroup. The

cycle repeats, generating oscillations in the membrane potentials of neurons (Buzsáki et al.,

2012).

The second model, termed the "E-I model," ascribes the generation of oscillations to the

feedback architecture between pyramidal cells and interneurons (Fiashn et al., 1998; Buzsáki et

al., 2012). The external excitation from mossy fibers and the perforant path recruits the

pyramidal neurons. The recurrent excitatory connections from the pyramidal neurons excite

interneurons. The interneurons then inhibit the pyramidal neurons, stopping them from firing.

Once the feedback inhibition in the network wears off, the pyramidal neurons begin firing again,

restarting the cycle.

Numerous studies have investigated the origin of gamma oscillations in the CA3 region.

Gamma oscillations can be induced *in vitro* via activation of muscarinic acetylcholine receptors

by carbachol (Fisahn et al., 1998; Mann et al., 2005; Zemankovics et al., 2013). Carbachol

induced gamma oscillations in the CA3 region were nullified following the administration of an

AMPA receptor antagonist (Fisahn et al., 1998). Application of a $GABA_A$ receptor antagonist

also abolished cholinergic gamma oscillations (Mann et al., 2005). Furthermore, pyramidal neurons fired around the trough of the oscillations, and interneurons fired on the ascending portion of the oscillations, following a short time lag (Hájos et al., 2004). The time lag between pyramidal neurons and interneurons was also observed *in vivo* (Csicsvari et al., 2003). These data suggest that both phasic excitation and inhibition are crucial in generating gamma oscillations. Therefore, the pyramidal-interneuron feedback loop is likely responsible for gamma oscillations in the CA3.

Modification of Gamma Oscillation Frequency

The frequency of network oscillations can be modified by network connectivity and synaptic dynamics. An *in vitro* study conducted by Mann and Mody (2010) investigated the increase in frequency of carbachol induced gamma oscillations in the CA3 region. They found that in wildtype rats, the oscillation frequency was around 40Hz. Upon genetic ablation of the δ-GABA$_A$ receptor however, the oscillation frequency increased to around 70Hz (Mann and Mody, 2010). They proposed that the δ-GABA$_A$ receptor mediates a tonic inhibitory current that inhibits the activation of NMDA receptors. Once the inhibition from δ-GABA$_A$ is removed, neurons become more sensitive to excitation from NMDA receptor mediated currents. The tonic excitation from NNDA receptors is hypothesized to shift the values for the instantaneous cycle frequencies to higher ranges. Furthermore, the authors observed a decrease in the phase lag and time lag between the firing of pyramidal neurons and interneurons during a given cycle (Mann and Mody, 2010). The exact mechanism of the reduction is unclear. One possibility is that the NMDA receptor mediated current reduces synaptic latencies by decreasing membrane time constants. Their data led them to conclude that this was not the case. Instead, the authors suggest that the tonic excitation from NMDA receptors allows interneurons to oscillate on their own,

setting a higher frequency for the network oscillations. This entails a shift in network behavior from the E-I model to the I-I model.

The purpose of this project was to investigate the underlying shift in network behavior in the modulation of gamma oscillation frequency by NMDA receptors. Various *in silico* studies have shown that inhibitory networks can oscillate on their own (Wang and Buzsáki, 1996; Vida et al., 2006; Mann and Paulsen, 2007). In this project, we built and tuned an integrate-and-fire model of the neurons in the CA3 region based on physiological data. Furthermore, we incorporated NMDA receptors in the model to study the mechanism behind the increase in frequency of gamma oscillations.

Methods

As shown in Fig. 1A, the network consists of two cell populations: excitatory pyramidal cells (PNs) and inhibitory interneurons (INs). The PN population consists of 200 neurons and the IN population consists of 50 neurons. In accordance with previous research, the network is sparsely and randomly connected (Börgers and Kopell, 2003; Buzsáki and Wang, 2012). The connections are made with specific cell-to-cell connection probabilities. The probability that a PN synapses onto another PN or IN is 0.05 and 0.15 respectively. The probability that an IN synapses onto a PN or another IN is 0.25 and 0.25 respectively.

The Integrate and Fire Model

$$\frac{dV}{dt} = -g_L(V) - g_{AMPA}(t)(V - E_{AMPA}) - g_{GABA}(t)(V - E_{GABA}) + I_{NMDA} + i_b$$

The above differential equation models the membrane potential of each neuron in the network. The model is based on a non-dimensionalized model of neurons in the visual cortex (Tao et al., 2004). The membrane potential, V, ranges from 0 to 1. The resting membrane

potential is zero. A membrane potential value of one indicates a neuron spike - an action potential. If $V \geq 1$, the time step at which the neuron spiked is recorded and the membrane potential is held at zero for 2.0ms, the length of the refractory period. When a presynaptic neuron spikes, postsynaptic cells receive a current following a latency period. As shown in Fig. 1B/C, when a PN spikes, postsynaptic cells receive excitatory currents mediated by AMPA and NMDA channels. When an IN spikes, postsynaptic cells receive an inhibitory current mediated by GABA channels.

The semipermeable nature of the membrane is represented by the $-g_L(V)$ term, where g_L is 0.05 ms^{-1}. This term causes a slow leak current that relaxes the membrane potential to zero. The $-g(t)(V - E)$ terms cause excitatory and inhibitory currents to increase and decrease the membrane potential respectively. The reversal potential, E, is the value of the membrane potential at which the current is equal to zero. In this model, the non-dimensionalized values for the reversal potentials for the AMPA and GABA currents are 4.67, and -0.67 respectively. The difference between the membrane potential and the reversal potentials, multiplied by the channel conductance as a function of time, $g(t)$, drives the flow of currents in the neuron. If a given neuron has k presynaptic inputs, the following sum describes the conductance for AMPA and GABA channels:

$$g_{\alpha,\beta}(t) = \sum_{i=1}^{k} A_{\alpha,\beta} \, \gamma_i \qquad \alpha\epsilon(PN,IN), \beta\epsilon(AMPA,GABA)$$

where

$$\gamma_i = \begin{cases} e^{\frac{-(t-(t_i^* + l_{\alpha,\beta}))}{\tau_{\alpha,\beta}}} & , \quad t \geq t_i^* + l_{\alpha,\beta} \\ \\ 0 & , \quad t < t_i^* + l_{\alpha,\beta} \end{cases}$$

A denotes the strength of the synaptic input. The non-dimensionalized strength of the AMPA and GABA current is 0.10 and 0.65 respectively. The indicator function γ_i denotes the contribution of the ith presynaptic neuron to the corresponding channel conductance. The term t_i^* indicates the spike time of the ith presynaptic neuron while t indicates the current time in the simulation. The addition of the l term simulates the synaptic latencies between specific cell-to-cell connections. The latency between a presynaptic PN and a postsynaptic PN and IN is 0.5ms and 1.8ms respectively. The latency between a presynaptic IN and a postsynaptic PN and IN is 0.6ms and 1.1ms respectively. If the current time in the simulation is greater than the presynaptic spike time with an added latency, γ_i is described by the negative exponential term. The synaptic input decays with a constant, τ, specific to cell-to-cell connections. The time constant denotes the time it takes for the strength of an input to reach roughly 66% of its initial value. The constant for input from a PN to PNs and INs is 1.7ms^{-1} and 1.6ms^{-1} respectively. The constant for input from an IN to PNs and INs is 3.3ms^{-1} and 1.2ms^{-1} respectively.

The classic model (Moradi et al., 2013) simulates the dynamics of the current mediated by NMDA channels.

$$I_{NMDA} = -g(B - A)Mg(V - E_{NMDA})$$

$$\frac{dA}{dt} = -\frac{A}{\tau_A}$$

$$\frac{dB}{dt} = -\frac{B}{\tau_B}$$

$$Mg = \frac{1}{(8 + e^{-8(v-0.6)})}$$

When a presynaptic PN spikes, the cell releases glutamate into the synapse, activating the NMDA channels. The channels activate and open quickly. A slow deactivation period follows, during which the channel closes. The result is a tonic, excitatory current (Banke et al., 2003). In

this model, g represents the maximal synaptic conductance of NDMA channels, non-dimensionalized to one. A and B govern the activation and deactivation of the NMDA channel respectively. Following a presynaptic PN spike, A and B are increased by constant factors. In PNs, the factors for activation and deactivation are $5.0e^{-5}$ and $1.1e^{-4}$ respectively. In INs, the factors for activation and deactivation are $7.0e^{-6}$ and $1.0e^{-5}$ respectively. The activation values decay with a fast time constant and the deactivation values decay with a slow time constant. The time constants for activation and deactivation are $2.8ms^{-1}$ and $65ms^{-1}$ respectively. The Mg term simulates the voltage dependent blocking of the NMDA channel by magnesium. Fig. 11 displays the non-dimensionalized equation for the magnesium block as a function of membrane potential of the neuron. The neurons also receive white noise background current, i_b, that simulates the external inputs from mossy fibers and the perforant path. The background current to PNs ranges from 0 to 0.17 whereas the background current to INs ranges from 0 to 0.01.

The following parameters in the model were found in literature: latency and τ from INs to PNs, latency and τ from INs to INs (Bartos et al., 2002), E_{AMPA}, E_{GABA}, and g_L(Tao et al., 2004). The rest of the parameters were tuned within physiological ranges.

The Simulation

The simulation, written in Python, runs with a 0.1ms time-step. Each time step consists of iterating through each neuron's synaptic inputs, and calculating the input to the synaptic conductance for AMPA, GABA and NMDA channels. The Euler method is used to analytically solve the membrane equation. At the end of the simulation, data are stored as json files and are processed using the SciPy and NumPy packages in Python, and MATLAB.

<div align="center">**Results**</div>

Gamma oscillations without NMDA

The CA3 network model simulated carbachol induced gamma oscillations without NMDA receptor activation as observed *in vitro* (Mann and Mody, 2010). Pyramidal neurons (PNs) and interneurons (INs) fired synchronously and regularly on each oscillation cycle (Fig. 2A). On average, PNs fired at 4.6 ± 5.6 spikes/second. INs fired much more frequently, at 18.9 ± 13.2 spikes/second (Fig. 2B). The INs fired with a short time lag after the PNs. A time lag of 4.3 ± 3.4ms was observed in the binned histogram of neuron spikes (Fig. 2C).

The synchronous firing of neurons caused the local field potential to oscillate at ~40Hz (Fig. 3A, bottom). The mean length of oscillation periods was 23.6 ± 4.9ms (Fig. 3A, top). Oscillations were also observed in the PN and IN field potentials. The PN field potential closely resembled the local field potential of all neurons, suggesting that PN activity set the oscillation periods, and therefore, the frequency. INs on the other hand, exhibited less oscillatory behavior, instead firing in a reactionary manner to PN activity (Fig. 3B). When each oscillation cycle was normalized to a $-\pi$ to π scale, a clear phase lag is present between PN and IN spikes.

Network behavior during gamma oscillations

During gamma oscillations, PNs exhibited subthreshold oscillations in their membrane potentials (Fig. 4A, left). PNs were depolarized mainly by input currents from mossy fibers and the perforant path, and hyperpolarized by bursts of $GABA_A$ mediated inhibition (Fig. 4A, left). INs also exhibited subthreshold oscillations, albeit at lower amplitudes. INs were depolarized by bursts of AMPA mediated excitation and hyperpolarized by $GABA_A$ mediated inhibition (Fig. 4A, right). PNs received significantly more inhibition than they did excitation. Conversely, INs received slightly more excitation than they did inhibition (Fig. 4B).

Both phasic excitation and inhibition are crucial for gamma oscillations

As shown in Fig. 5A (top), gamma oscillations were no longer present following removal of AMPA receptors. This simulated the nullification of gamma oscillations following application of an AMPA receptor antagonist (Mann and Mody, 2010). A small peak at ~50Hz was present in the power spectrum of the local field potential (Fig. 5A, bottom). This was most likely due to PNs being depolarized by the tonic excitation from mossy fibers, and then being relaxed to resting membrane potential by the leak current. As shown in Fig. 5A (middle), without AMPA mediated excitation, INs did not spike. Therefore, the only way PNs could have been hyperpolarized was via the leak current. Furthermore, removing $GABA_A$ receptors also abolished oscillations in the local field potential (Fig. 5B, top, bottom). The IN field potential exhibited oscillatory behavior due to the uninhibited excitation to the INs that caused them to fire continuously (Fig. 5B, middle). This suggests that AMPA receptor mediated phasic excitation and $GABA_A$ mediated phasic inhibition are both necessary for gamma oscillations.

Increased oscillation frequency due to NMDA receptor mediated excitation

Consistent with *in vitro* observations, activation of NMDA receptors increased the frequency of gamma oscillations to the ~50-70Hz range (Fig. 6B, bottom). Following activation of NMDA receptors, the firing rates of both PNs and INs increased (Fig. 6A, left). On average, PNs spiked 6.5 ± 15.2 times per second while INs spiked 35.9 ± 28.1 times per second. The increased IN firing rate reflects the increased *in vitro* post synaptic inhibitory current activity following NMDA receptor activation (Mann and Mody, 2010). Binned spike time histograms (Fig. 6A, right), and field potentials of PNs and INs (Fig. 6C, top) showed a decreased time lag between the PN and IN populations. As shown in Fig. 6C (bottom), activation of NMDA

receptors caused the time lag between PNs and INs to decrease. The mean time lag between PN

and IN spikes was 2.8 ± 0.9ms.

The power spectrum of the local field potential showed a broad peak in the higher

frequency ranges. This was indicative of greater variation in oscillation cycle frequencies as seen

in Fig. 8A. The binned histogram of instantaneous cycle frequencies showed a broader peak

centered at ~70Hz with active NMDA compared to a sharp peak at ~40Hz without active

NMDA. This shows the model accurately simulates the NMDA receptor activation mediated

increase in oscillation frequency observed *in vitro*.

Shift in excitation/inhibition balance following NMDA receptor activation

Activation of NMDA receptors caused a tonic, excitatory current to depolarize both PNs

and INs (Fig. 7A, top; Fig. 7B, top). The tonic excitation caused the period of subthreshold

oscillations to decrease in PNs (Fig. 7A, top). Activation of NMDA receptor mediated current

caused the PNs to receive much more AMPA receptor mediated excitation, due to recurrent PN-

PN connections observed *in vivo* (Bains et al., 1999). Compared to their inputs without NMDA

receptor activity, INs also received more AMPA mediated excitation. The overall excitation and

inhibition in the network were more balanced following NMDA activation as seen *in vitro*

(Mann and Mody, 2010). Furthermore, an inverse relationship between net NMDA receptor

mediated current and instantaneous cycle frequency was observed (Fig. 8B). The cycles with

lower frequencies exhibited higher activation of NMDA receptors in both PNs and INs (Fig. 8C).

These findings suggest that a change in the balance between excitation and inhibition causes a

rise in the oscillation frequency.

IN network oscillations following removal of PN-IN AMPA mediated feedback

When the PN-IN AMPA mediated current were removed from the network, INs displayed distinct oscillatory behavior (Fig. 9A). The tonic excitation from NMDA mediated currents caused the INs to oscillate on their own. PNs did not oscillate, presumably due to the decreased inhibition from the less active INs. Therefore, oscillations in the local field potential were not apparent (Fig. 9A). When both PN-IN AMPA and NMDA mediated currents were removed, INs stopped firing, resulting in a flat IN field potential (Fig. 9B, top). The PNs continued to exhibit low amplitude oscillatory behavior simply due to the background current (Fig. 9B, top). Therefore, a small peak in the power spectrum was observed in both the PN and the local field potential (Fig. 9B, bottom).

Selective activation of NMDA receptors on PNs and INs

In vitro observations showed that the NR2D subunit-containing NMDA receptor were located on just INs (Mann and Mody, 2010). This is not to say that NMDA mediated currents are not active on PNs, as receptors containing other subunits have been observed in CA3 PNs (Nakazawa et al., 2002; Nakazawa et al., 2003). To test the necessity of NMDA activation on PNs for the generation of higher frequency oscillations, NMDA receptors were selectively expressed on PNs and INs. When NMDA receptors were on just PNs, the oscillation frequency increased to ~50Hz. When NMDA receptors were only on INs, the oscillation frequency decreased to the 40Hz range. These findings suggest that tonic excitation to PNs is necessary for the increase in gamma oscillation frequency.

Discussion

The model revealed that without NMDA receptors, gamma oscillations are generated via a feedback loop between PNs and INs. The PN field potential closely resembles the local field potential of the entire network, suggesting that PN activity determines oscillations in the network. Furthermore, INs fire synchronously with a time lag after PNs fire. PNs receive much more inhibition than excitation, whereas INs receive more excitation than they do inhibition. This shows that PNs synchronously excite the INs, which fire in response, inhibiting the PNs. Once the inhibition wears off, the PNs fire again, restarting the cycle. As seen in Fig.5, removing either AMPA or GABA$_A$ synapses from the model abolishes the gamma oscillations. Without AMPA receptors, the PNs are no longer capable of exciting the INs, and the feedback loop is destroyed. Without GABA$_A$ receptors, INs cannot inhibit PNs, and therefore the loop is cut off and oscillations disappear. These findings show that the underlying mechanism of non-NMDA gamma oscillations is the PN-IN feedback loop.

As seen *in vitro* (Mann and Mody, 2010), the activation of NMDA receptors increases the frequency of gamma oscillation. Furthermore, the time lag between PNs and INs decreases. The instantaneous cycle frequency histograms also show that activation of NMDA causes a wider distribution of cycle frequencies, suggesting that the mechanism of oscillation generation is not homogenous. We propose that NMDA receptor mediated increase in oscillation frequency caused by a shift from the PN-IN feedback loop to IN-IN intranetwork oscillations. The decreased time lag between PN and IN spikes suggests that INs no longer need PN spikes to depolarize them. Instead, the tonic currents from NMDA receptor channels excite INs. When the INs fire, they inhibit each other. Once the inhibition wears off, the tonic currents excite INs

again, and the cycle restarts. Increased firing rates of INs supports this idea, as the intranetwork oscillation scheme would require increased IN activity to maintain oscillations.

To test the idea of a mechanistic shift, we removed PN-IN AMPA synapses from the network. This effectively removed the ability of the PNs to quickly excite INs, blocking the PN-IN feedback loop. INs displayed distinct oscillatory behavior in their field potential, while PNs did not. When we removed NMDA receptors as well as PN-IN AMPA synapses from the network, INs ceased to oscillate. These results show that in the absence of PN-IN feedback, tonic excitation from NMDA receptors causes INs to oscillate on their own.

One would expect that if NMDA receptor activation increases oscillation frequency, then more NMDA receptor mediated current would be active during cycles that exhibit higher instantaneous oscillation frequencies. Interestingly, we found a negative correlation between net NMDA mediated current and instantaneous oscillation frequency. We suggest that the ratio of NMDA activation in PNs and INs is responsible for the discrepancy. When we ran simulations with NMDA receptors on only PNs, the oscillation frequency increased. Conversely, when NMDA receptors were present on just INs, the frequency decreased. Perhaps in cycles that exhibit high instantaneous frequencies, the ratio of NMDA mediated excitation to PNs versus INs is higher. Conversely, in cycles that exhibit lower instantaneous frequencies, the ratio of NMDA mediated excitation to PNs versus INs is lower. Further study of the balance of NMDA mediated excitation is necessary to fully understand the inverse relationship between NMDA mediated excitation and instantaneous oscillation frequency.

Conclusion

In summary, our simulations showed that without NMDA mediated excitation, the PN-IN feedback loop is responsible for gamma oscillations. Our findings suggest that NMDA receptor activation increases the frequency of gamma oscillations by shifting the mechanism towards IN-IN intranetwork oscillations. Moreover, the balance of NMDA mediated excitation to pyramidal neurons and interneurons may control the instantaneous cycle frequencies in the oscillations. Further study of mechanism shift and the balance of NMDA mediated excitation is important to fully understand the modulation of gamma oscillation frequency.

Figures
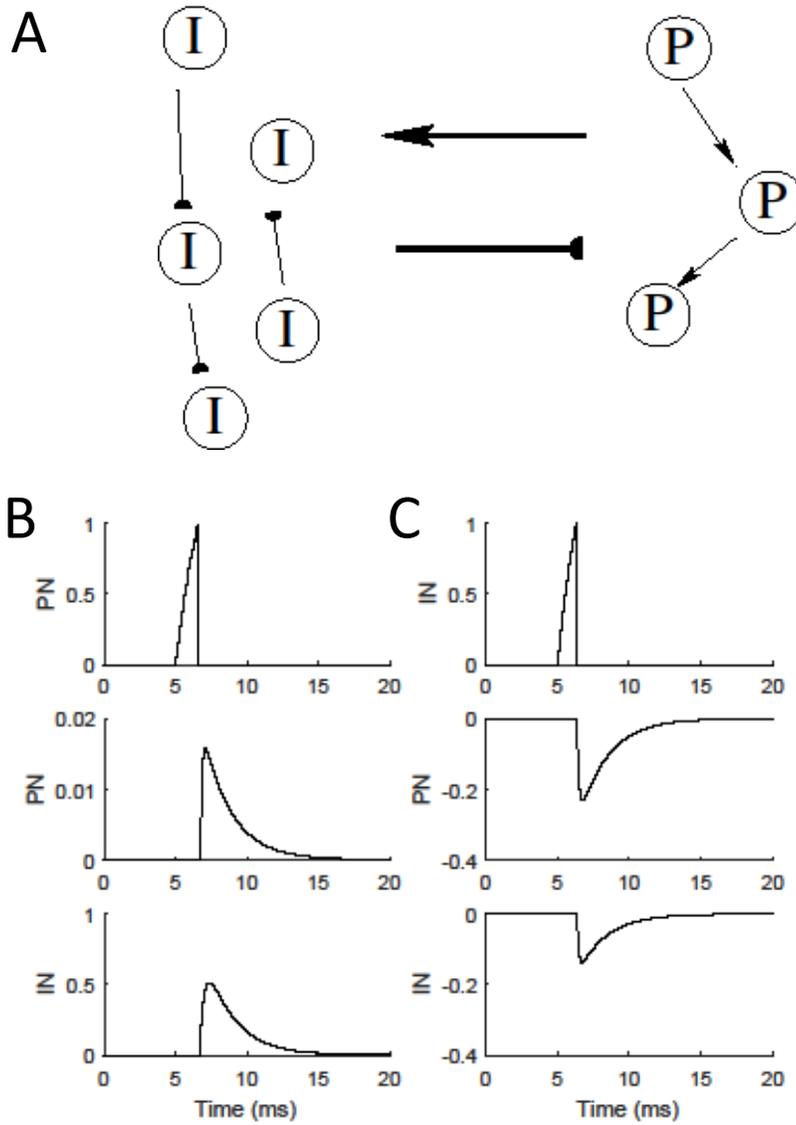
Figure 1. Network organization and neuron behavior. A, the PN-IN feedback loop. B, when a PN spikes (top), post synaptic PNs(middle) and INs(bottom) receive excitatory currents that decay over time. C, when an IN spikes (top), post synaptic PNs (middle) and INs (bottom) receive inhibitory currents that decay over time.
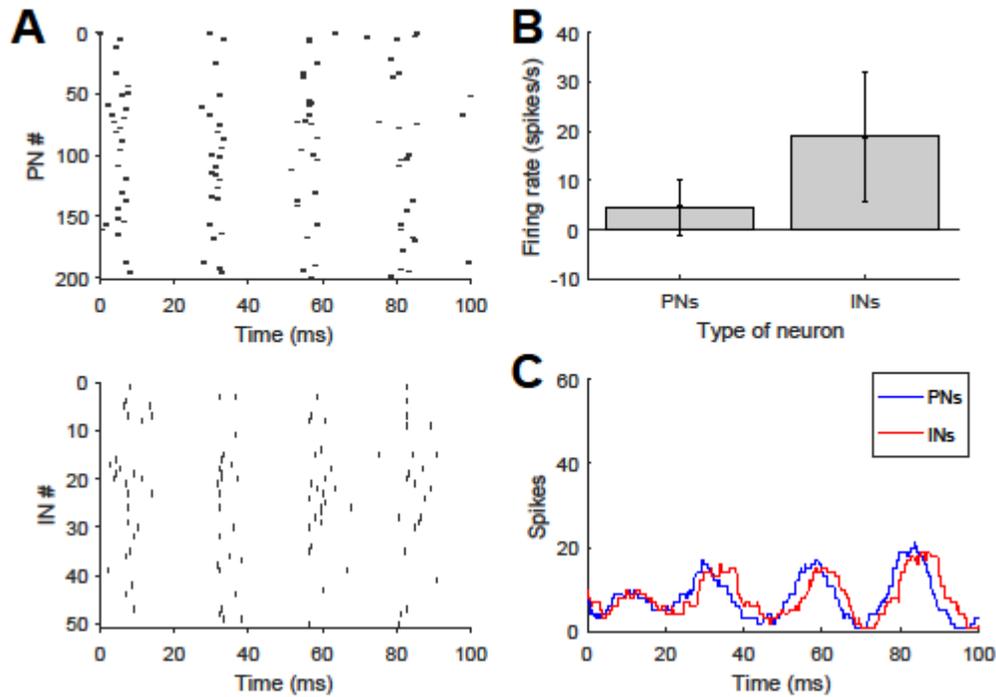
Figure 2. Firing pattern summaries of neurons in simulated CA3 region of hippocampus. A, spike rasters of PNs (top) and INs (bottom). B, mean firing rates of PN and IN populations. PNs exhibited a mean firing rate of 4.6 ± 5.6 spikes/s. INs exhibited a mean firing rate of 18.9 ± 13.2 spikes/s. Mean population firing rates were calculated by averaging mean firing rates of individual neurons over a 1600ms simulation. C, binned histogram of PN and IN spikes with a bin size of 5ms. The mean time lag between PN and IN spikes was 4.3 ± 3.4ms, calculated over 69 cycles. Mean time lag was calculated by convolving both PN and IN spike counts with a Gaussian filter and averaging the peak-to-peak time differences over 69 cycles.
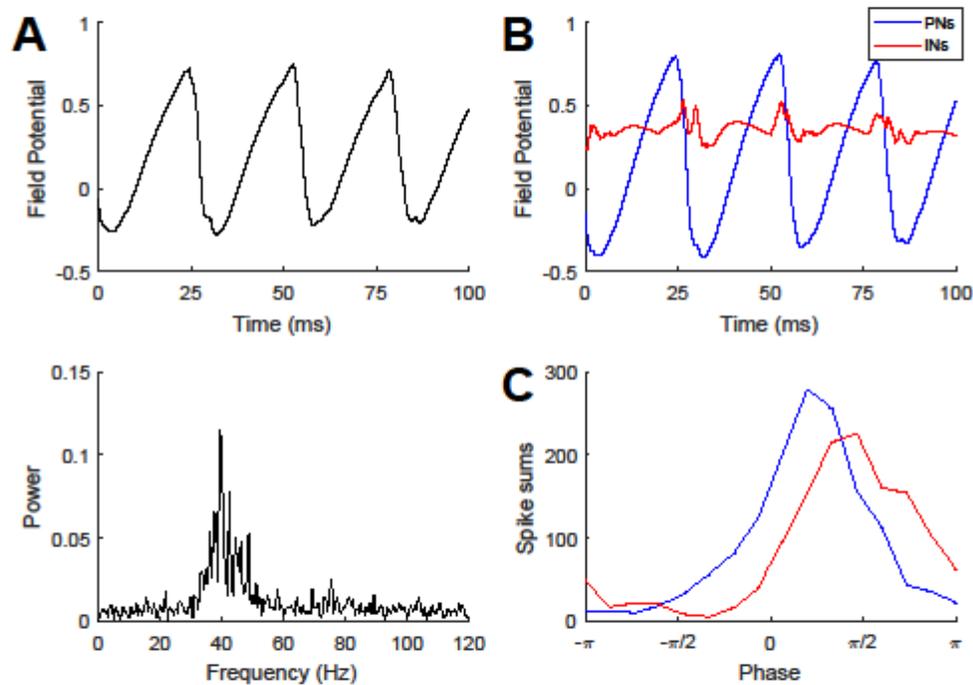
Figure 3. Gamma oscillations emerge in network without NMDA. A, local field potential calculated by averaging the membrane potentials of all neurons at each time step (top).The mean period length was 23.6 ± 4.9ms, calculated by convolving the local field potential with a Gaussian filter and averaging the peak-to-peak time differences in the local field potential over 65 cycles. The corresponding power spectrum of the local field potential (bottom). B, the field potential of PNs and INs, calculated by averaging the membrane potentials of all PNs and INs respectively, over a 1600ms simulation. C, the sum of PN and IN spikes in each oscillation period, normalized to a -π to π scale with a bin size of π/8. Spikes were summed over 65 cycles.
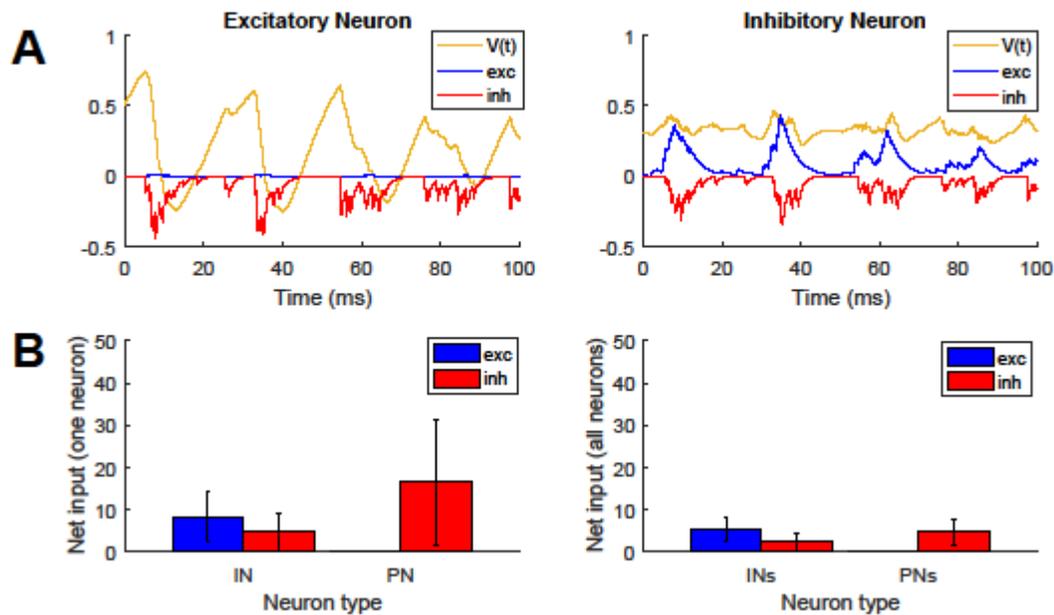
Figure 4. Neuron inputs in simulated network. A, membrane potential, exc (AMPA mediated) and inh (GABA_A mediated) current of one PN (left) and one IN (right) over a 100ms period. B (left), mean exc and inh current to one randomly chosen PN/IN, calculated by averaging the net integral of each current to one neuron over 39 oscillation cycles. B (right), the mean exc and inh current to all PNs and all INs in one randomly chosen oscillation cycle calculated by averaging the net integral of each current to all PNs and INs in the chosen cycle.
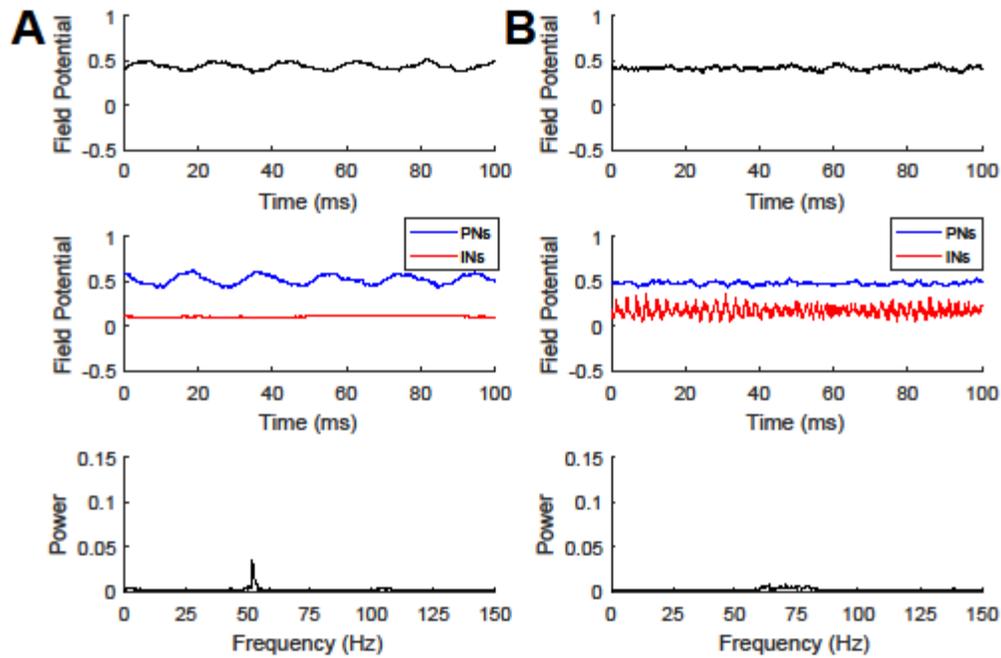
Figure 5. Network behavior without AMPA and GABA$_A$ mediated currents. Local field potential (top), PN/IN field potentials (middle), and power spectrum (bottom) of the local field potential in a network lacking AMPA (A) and GABA$_A$ mediated (B) currents. Local field potential was calculated by averaging the membrane potentials of all neurons in network at each time step. PN and IN field potentials were calculated by averaging the membrane potentials of all PNs and INs respectively, at each time step.
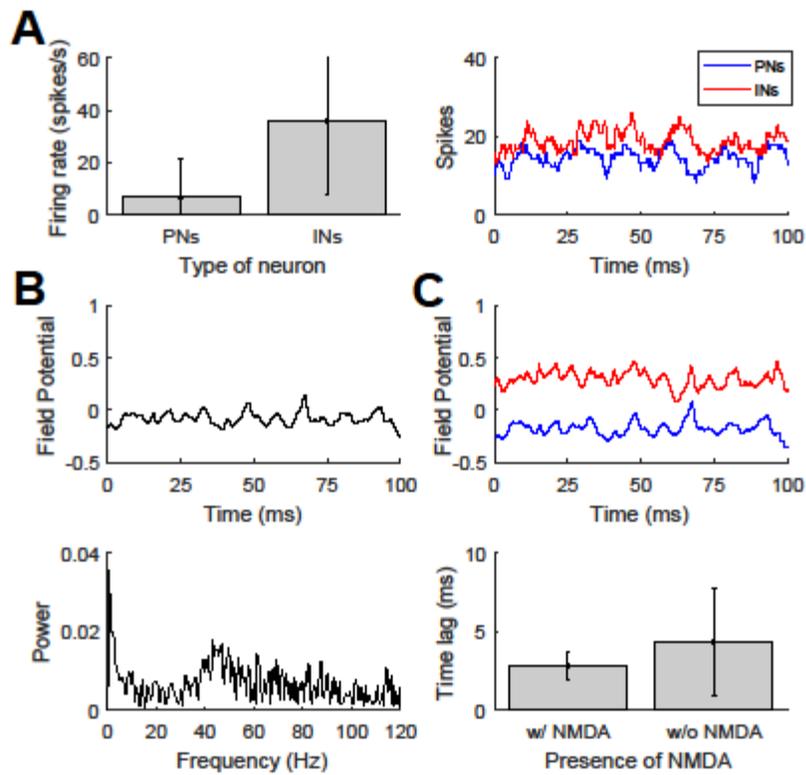
Figure 6. Network behavior with NMDA currents. A, mean firing rates (left) and binned histogram of spike counts (right) of PNs and INs, with a 5ms bin size. B, Total field potential (top) and corresponding power spectrum (bottom) of the network. C, PN and IN field potentials (top), and time lag between PN and IN spikes (bottom). Time lag was calculated by convolving the PN and IN spike counts with a Gaussian, and averaging the peak-to-peak time differences over 66 cycles.
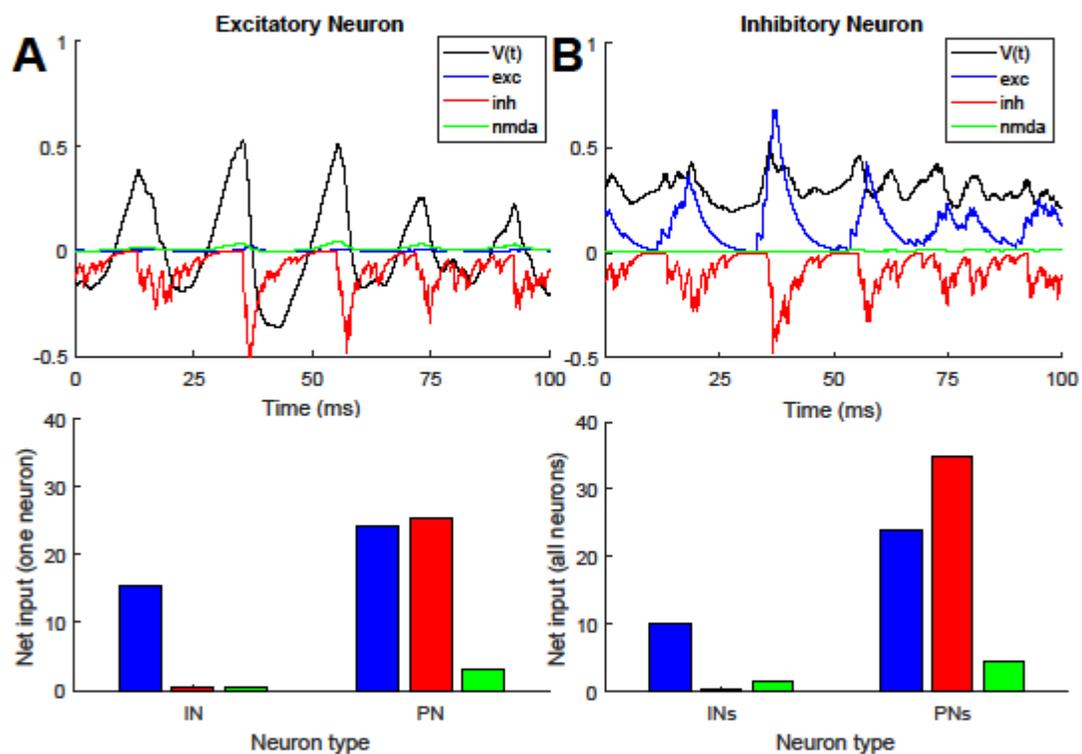
Figure 7. Neuron behavior with active NMDA currents. A, Membrane potential, exc (AMPA mediated), inh (GABA$_A$ mediated), and NMDA mediated inputs to a randomly chosen PN. B, Membrane potential, exc, inh, and NMDA mediated inputs to a randomly chosen IN. C, Net exc, inh, NMDA currents to one random neuron in the network (left), and to all neurons in the network (right) over the course of a 1600ms simulation. Net exc, inh, and NMDA currents were calculated by integrating the exc, inh, and NMDA inputs respectively.
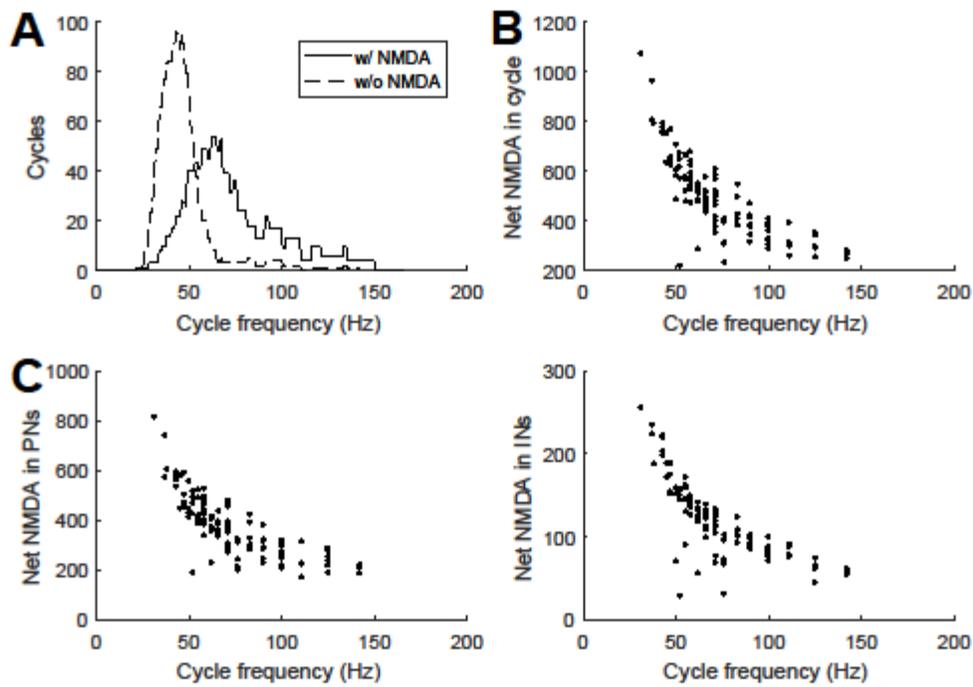
Figure 8. Instantaneous cycle frequencies. A, binned histogram of instantaneous cycle frequencies in a network with active NMDA current (solid line, calculated over 120 cycles with bin size of 10 Hz) and without active NMDA current (dashed line, calculated over 123 cycles, with bin size of 10 Hz). B, the net integrated NMDA current in each cycle as a function of cycle frequency, in the entire network, calculated over 137 cycles. C, the net integrated NMDA input to PNs (left) and INs (right) in each cycle as a function of cycle frequency, calculated over 137 cycles.
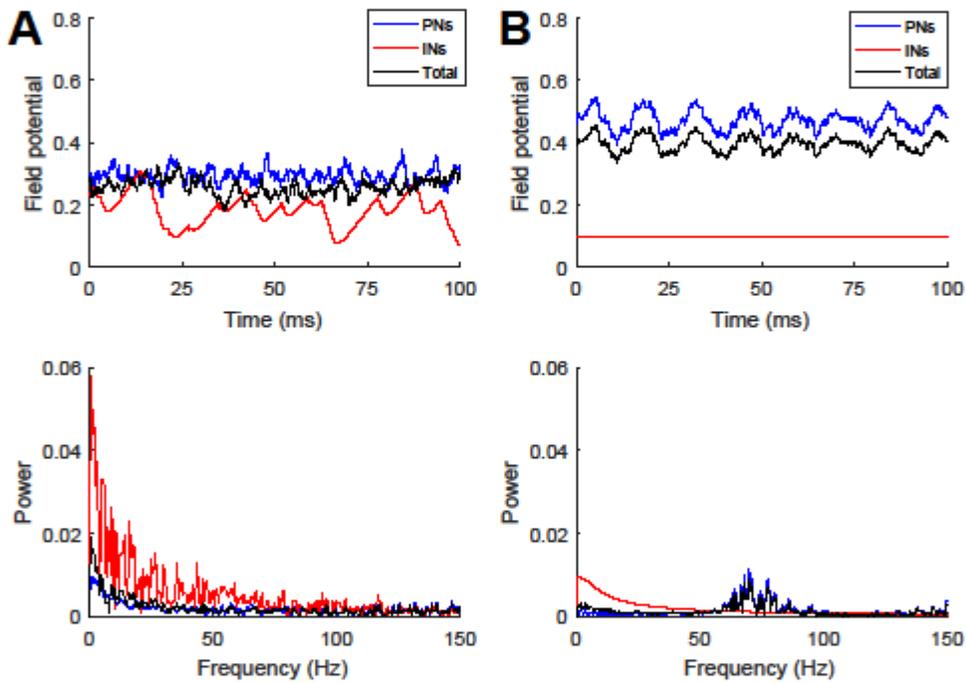
Figure 9. Network behavior without PN-IN AMPA feedback. Simulations were ran after removing AMPA synapses between PNs and INs. A, network behavior with active NMDA current. PN, IN, and total field potentials (top) and respective power spectra (bottom). B, network behavior without active NMDA current. PN, IN, and total field potentials (top) and respective power spectra (bottom). The PN, IN, and total field potentials were calculated by averaging the membrane potential for the PNs, INs, and all cells respectively, at each time step.
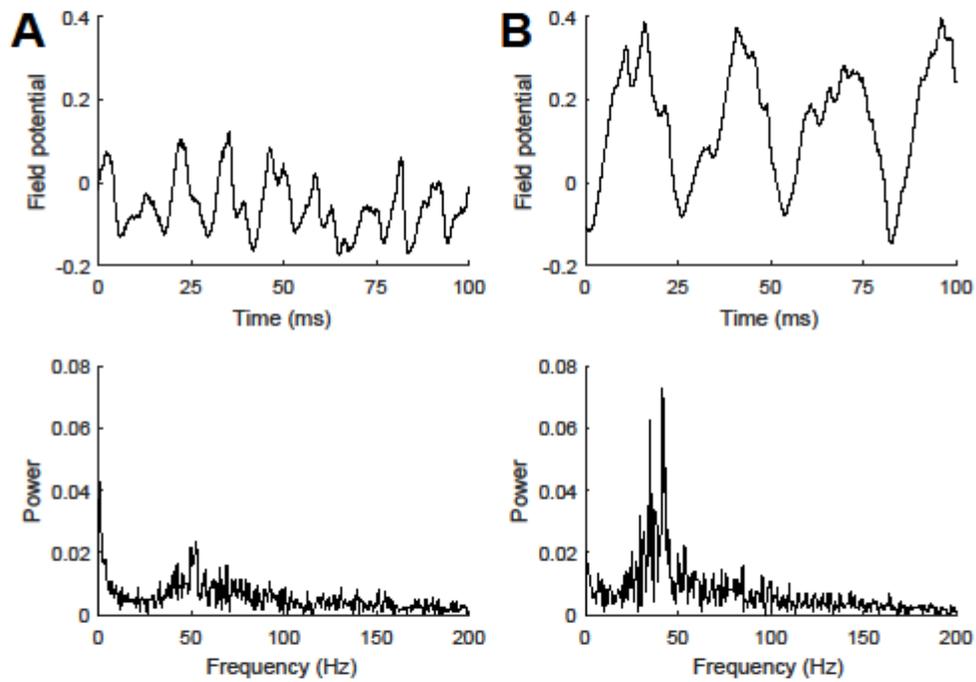
Figure 10. Network oscillations with selective NMDA expression. A, NMDA receptor expressed only on PNs and B, NMDA receptor expressed only on INs. Local field potential (top) calculated by averaging the membrane potential of all cells at each time step and corresponding power spectrum (bottom).
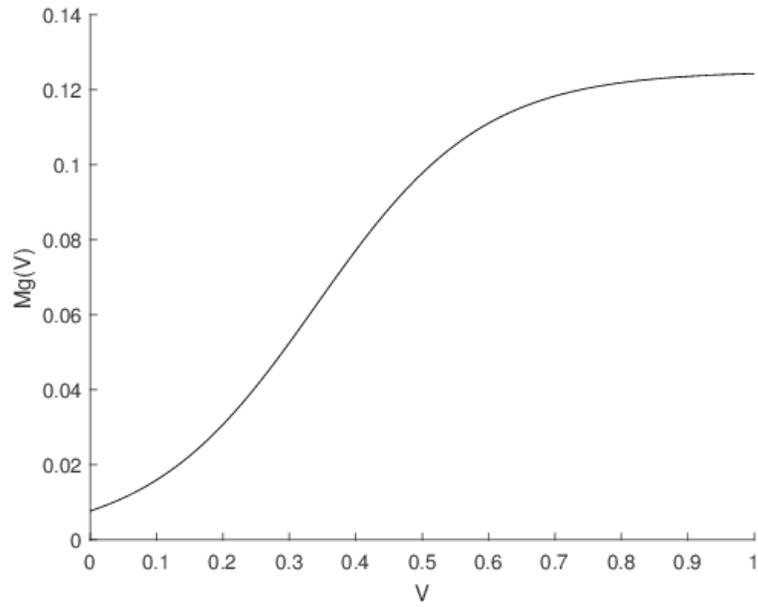
Figure 11. The magnesium block as a function of membrane potential. The non-dimensionalized equation for the magnesium block is as follows: $Mg = \dfrac{1}{\left(8 + e^{-8(v-0.6)}\right)}$

References

Andersen, P., Morris, R., Amaral, D., Bliss, T., & O'Keefe, J. (2007). *The Hippocampus Book.* New York, New York: Oxford University Press.

Bains, J. S., Longacher, J. M., & Staley, K. J. (1999). Reciprocal interactions between CA3 network activity and strength of recurrent collateral synapses. *Nature Neuroscience, 2*(8), 720-726.

Banke, T. G., & Traynelis, S. F. (2003). Activation of NR1/NR2B NMDA receptors. *Nature Neuroscience, 6*(2), 144-152.

Bartos, M., Vida, I., Frotscher, M., Meyer, A., Monyer, H., Geiger, J. R. P., & Jonas, P. (2002). Fast synaptic inhibition promotes synchronized gamma oscillations in hippocampal interneuron networks. *Proceedings of the National Academy of Sciences, 99*(20), 13222-13227.

Bartos, M., Vida, I., Jonas, P. (2007). Synaptic mechanisms of synchronized gamma oscillations in inhibitory interneuron networks. *Nature Reviews Neuroscience, 8*(1), 45-56.

Bauer, M., Oostenveld, R., Peeters, M., & Fries, P. (2006). Tactile spatial attention enhances gamma-band activity in somatosensory cortex and reduces low-frequency activity in parieto-occipital areas. *Journal of Neuroscience*, *26*(2), 490-501.

Börgers, C., & Kopell, N. (2003). Synchronization in networks of excitatory and inhibitory neurons with sparse, random connectivity. *Neural computation, 15*(3), 509-538.

Börgers, C., & Kopell, N. J. (2008). Gamma oscillations and stimulus selection. *Neural computation, 20*(2), 283-414.

Brunel, N., & Wang, X. J. (2003). What determines the frequency of fast network oscillations with irregular neural discharges? I. Synaptic dynamics and excitation-inhibition balance. *Journal of Neurophysiology, 90*(1), 415-430.

Busch, N. A., Debener, S., Kranczioch, C., Engel, A. K., & Herrmann, C. S. (2004). Size matters: effects of stimulus size, duration and eccentricity on the visual gamma-band response. *Clinical Neurophysology, 115*(8), 1810-1820.

Buzsáki, G., & Draguhn, A. (2004). Neuronal oscillations in cortical networks. *Science, 304*, 1926-1929.

Buzsáki, G., & Wang, X.J. (2012). Mechanisms of gamma oscillations. *Annual Review of Neuroscience, 35,* 203-225.

Colgin, L. L., Denninger, T., Fyhn, M., Hafting, T., Bonnevie, T., Jensen, O., Moser, M. B., & Moser, E. I. (2009). Frequency of gamma oscillations routes flow of information in the hippocampus. *Nature, 462*, 352-357.

Cherubini, E., & Miles, R. (2015). *The CA3 Region of the Hippocampus: How is it? What is it for? How does it do it?* Lausanne: Frontiers Media.

Csicsvari, J., Jamieson, B., Wise, K. D., & Buzsáki, G. (2003). Mechanisms of gamma oscillations in the hippocampus of the behaving rat. *Neuron*, *37*(2), 311-322.

Cull-Candy, S., Brickley, S., & Farrant, M. (2001). NMDA receptor subunits: diversity, development and disease. *Current Opinion in Neurobiology, 11*(3), 327-335.

Fisahn, A., Pike, F. G., Buhl, E. H., & Paulsen, O. (1998). Cholinergic induction of network oscillations at 40 Hz in the hippocampus in vitro. *Nature, 394*(6689), 186-189.

Geiger, J. R. P., Lübke, J., Roth, A., Frotscher, M., & Jonas, P. (1997). Submillisecond AMPA receptor-mediated signaling at a principal neuron-interneuron synapse. *Neuron, 18*(6), 1009-1023.

Hájos, N., Pálhalmi, J., Mann, E. O., Németh, B., Paulsen, O., & Freund, T. F. (2004). Spike timing of distinct types of GABAergic interneuron during hippocampal gamma oscillations in vitro. *The Journal of Neuroscience, 24*(41), 9127-9137.

Hájos, N., & Paulsen, O. (2009). Network mechanisms of gamma oscillations in the CA3 region of the hippocampus. *Neural Networks*, *22*(8), 1113-1119.

Hasselmo, M. E., Schnell, E., & Barkai, E. (1995). Dynamics of learning and recall at excitatory recurrent synapses and cholinergic modulation in rat hippocampal region CA3. *The Journal of Neuroscience, 15*(7), 5249-5262.

Honkanen, R., Rouhinen, S., Wang, S. H., Palva, J. M., & Palva, S. (2014). Gamma oscillations underlie the maintenance of feature-specific information and the contents of visual working memory. *Cerebral Cortex, 25*(10), 3788-3801.

Howard., M. W., Rizzuto, D. S., Caplan, J. B., Madsen, J. R., Lisman, J., Aschenbrenner-Scheibe, R., Schulze-Bonhage, A., & Kahana, M. J. (2003). Gamma oscillations correlate with working memory load in humans. *Cerebral Cortex, 13*(12), 1369-1374.

Lasztóczi, B., & Klausberger, T. (2014). Layer-specific GABAergic control of distinct gamma oscillations in the CA1 hippocampus. *Neuron*, *81*(5), 1126-1139.

MacDonald, R. L. & Olsen, R. W. (1994). GABA$_A$ receptor channels. *Annual Review of Neuroscience, 17*(1), 569-602.

MacDonald, R. L., Rogers, C. J., & Twyman, R. E. (1989). Kinetic properties of the $GABA_A$ receptor main conductance state of mouse spinal cord neurones in culture. *Journal of Physiology, 410*, 479-499.

Mann, E. O., Suckling, J. M., Hájos, N., Greenfield, S. A., & Paulsen, O. (2005). Perisomatic feedback inhibition underlies cholinergically induced fast network oscillations in the rat hippocampus in vitro. *Neuron, 45*(1), 105-117.

Mann, E. O., & Paulsen, O. (2007). Role of GABAergic inhibition in hippocampal network oscillations. *Trends in Neuroscience, 30*(7), 343-349.

Mann, E. O., & Mody, I. (2010). Control of hippocampal gamma oscillation frequency by tonic inhibition and excitation of interneurons. *Nature Neuroscience, 13*(2), 205-212.

McBain, C. J., & Dingledine, R. (1993). Heterogeneity of synaptic glutamate receptors on CA3 stratum radiatum interneurons of rat hippocampus. *Journal of Physiology, 462*(1), 373-392.

Miles, R., Traub, R. D., & Wong, R. K. S. (1988). Spread of synchronous firing in longitudinal slices from the CA3 region of the hippocampus. *Journal of Neurophysiology, 60*(4), 1481-1496.

Möhler, H. (2006). $GABA_A$ receptor diversity and pharmacology. *Cell Tissue Research, 326*(2), 505-516.

Montgomery, S. M., & Buzsáki, G. (2007). Gamma oscillations dynamically couple hippocampal CA3 and CA1 regions during memory task performance. *Proceedings of the National Academy of Sciences*, *104*(36), 14495-14500.

Monyer, H., Burnashev, N., Laurie, D. J., Sakmann, B., & Seeburg, P. H. (1994). Developmental and regional expression in the rat brain and functional properties of four NMDA receptors. *Neuron, 12*(3), 529-540.

Moradi, K., Moradi, K., Ganjkhani, M., Hakhasani, M., Gharibzadeh, S., & Kaka, G., (2013). A fast model of voltage-dependent NMDA receptors. *Journal of Computational Neuroscience, 34*(3), 521-531.

Nakazawa, K., Quirk, M. C., Chitwood, R. A., Watanabe, M., Yeckel, M. F., Sun, L. D., Kato, A., Carr, C. A., Johnston, D., Wilson, M. A., & Tonegawa, S. (2002). Requirement of hippocampal CA3 NMDA receptors in associative memory recall. *Science, 297*(5579), 211-218.

Nakazawa, K., Sun, L. D., Quirk, M. C., Rondi-Reig, L., Wilson, M. A., & Tonegawa, S. (2003). Hippocampal CA3 NMDA receptors are crucial for memory acquisition of one-time experience. *Neuron, 38*(2), 305-315.

Sederberg, P. B., Schulze-Bonhage, A., Madsen, J. R., Bromfield, E. D., McCarthy, D. C., Brandt, A., Tully, M. S., & Kahana, M. J. (2007). Hippocampal and neocortical gamma oscillations predict memory formation in humans. *Cerebral Cortex, 17*(5), 1190-1196.

Sprutson, N., Jonas, P., Sakmann, B. (1995). Dendritic glutamate   receptor channels in rat hippocampal CA3 and CA1 pyramidal neurons. *Journal of Physiology, 482*(2), 325-352.

Tao, L., Shelley, M., McLaughlin, D., & Shapley, R. (2004). An egalitarian network model for the emergence of simple and complex cells in visual cortex. *Proceedings of the National Academy of Sciences, 101*(1), 366-371.

Tallon-Baudry, C., & Bertrand, O. (1999). Oscillatory gamma activity in humans and its role in object representation. *Trends in Cognitive Sciences*, *3*(4), 151-162.

Wang, X. J., & Buzsáki, G. (1996). Gamma oscillation by synaptic inhibition in a hippocampal interneuron network model. *Journal of Neuroscience, 16*(20), 6402-6413.

Vida, I., Bartos, M., & Jonas, P. (2006). Shunting inhibition improves robustness of gamma oscillations in hippocampal interneuron networks by homogenizing firing rates. *Neuron, 49*(1), 107-117.

Whittington, M. A., Traub, R. D., Kopell, N., Ermentrout, B., & Buhl, E. H. (2000). Inhibition-based rhythms: experimental and mathematical observations on network dynamics. *International Journal of Psychophysiology, 38*(3), 315-336.

Witter, M. P. (2007). Intrinsic and extrinsic wiring of CA3: indications for connectional heterogeneity. *Learning & Memory*, *14*(11), 705-713.

Wittner, L., Henze, D. A., Záborszky, L., & Buzsáki, G. (2006). Hippocampal CA3 pyramidal cells selectively innervate aspiny interneurons. *Europeran Journal of Neuroscience, 24*(5), 1286-1298.

Zemankovics, R., Veres, J. M., Oren, I., & Hájos, N. (2013). Feedforward inhibition underlies the propagation of cholinergically induced gamma oscillations from hippocampal CA3 to CA1. *Journal of Neuroscience*, *33*(30), 12337-12351.